

Tunable Doping and Characterization of Single-Wall Carbon Nanotube Macrosystems for Electrode Material Applications

Alexander A. Tonkikh,* Valentina A. Eremina, Ekaterina A. Obraztsova, Dmitry A. Musatov, Alexander Yu. Pereyaslavtsev, Esko I. Kauppinen, and Elena D. Obraztsova



Cite This: *ACS Appl. Nano Mater.* 2021, 4, 3220–3231



Read Online

ACCESS |



Metrics & More



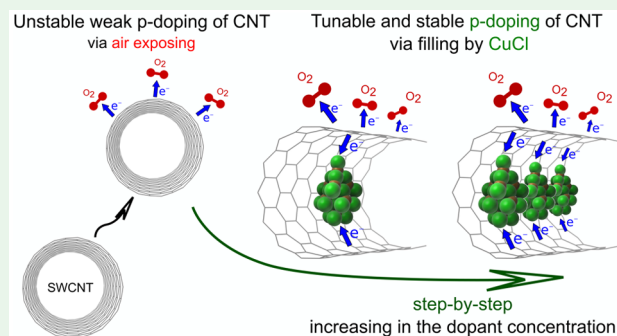
Article Recommendations



Supporting Information

ABSTRACT: We present an efficient method for easy tuning of optical and electrophysical parameters of macroscopic objects formed from single-wall carbon nanotubes (SWCNTs). We have developed a unique step-by-step doping procedure by filling the SWCNT inner channels with acceptors and donors in gaseous conditions. The main parameter that tailors the film properties is the dopant concentration in the SWCNT channels varied through the gaseous filling time. The ambient oxygen impact on the doping level has been measured and analyzed for all considered SWCNT objects. Our approach provides a predictable shift of Fermi level position in the range of 0.1–0.9 eV and the optical band gap edge value between 0.4 and 1.1 eV. The tuning method was applied to optimize the thermopower performance of SWCNT films. We have measured the maximum possible values of the power factor and thermoelectric coefficient and studied the stability of these parameters in the air for studied samples. On the basis of the revealed relation between thermopower and sheet resistance, we propose a general approach for characterization of conducting CNT macro-objects, which we call the “doping map” plotting. This empirical method allows to predict stable, maximum, or optimal values for the transport, thermopower, and optical characteristics of materials in the air. Our findings are prospective for prediction and tailoring of SWNT-containing materials properties used in such technological applications, as electrochemical, sensor, solar cell, or thermoelectric electrode materials.

KEYWORDS: carbon nanotube, encapsulation, nanotube filling, tunable doping, thermopower, air environment



1. INTRODUCTION

Carbon nanotubes are unique nanostructures studied for almost three decades. This is primarily due to interesting electrophysical properties, such as ballistic electron transport observed in individual defect-free nanotubes.¹ This material is also interesting from the point of view of its nonlinear optical properties used in optoelectronics.^{2–4} Recently, the CNT-oriented activity shifted from basic research to technological applications. In particular, there are several examples of successful applications of nanotubes as a functional material for transistors and sensors.^{5–7} In this case, they form macro-objects usually based on networks of as-synthesized nanotubes or hybrids of nanotubes with other materials. However, maintenance of the original outstanding properties of nanotubes in micro- and macrosystems remains challenging.

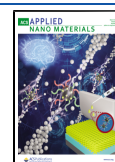
At the moment, the modification of macro- and micro-objects based on nanotube properties and the production of hybrid systems are rapidly developing trends. The modification methods include production of systems based on nanotubes of certain geometries and types of conductivity,⁸ various types of doping and functionalization,^{9–11} macro- and micro-objects morphology change;^{12,13} as well as the production of hybrid

systems where nanotubes can play the role of both the matrix and the functional material.¹³ These methods are primarily aimed to improve just one single parameter of nanotubes. However, it is often important to improve and to tune multiple characteristics of a functional material within the framework of a single technique. For macro-objects based on carbon nanomaterials, tuning is required for the position of the Fermi level, the work function (WF) of the material, and therefore, the optical density and transport characteristics.^{14–17} Control of these properties is necessary for various electronic and optoelectronic devices, such as organic field-effect transistors (OFETs), organic photovoltaic systems, sensors, and heterostructures.^{18,19} The technological methods for tuning the characteristics of micro- and macro-objects in most cases are based on the deposition of active substances on the surface of nanotubes or other

Received: February 9, 2021

Accepted: March 2, 2021

Published: March 12, 2021



nanomaterials.^{14,16,20} However, these approaches lead to material contamination, making them difficult to use.

In this paper, we consider two important issues. First, we demonstrate a way, allowing the formation of a material with adjusted Fermi level, WF, and electrophysical characteristics within one approach. We have developed a methodology for adjusting the electrophysical properties based on tuning of concentration and type of dopant in the channels of carbon nanotubes. The technique of filling the internal channels with a doping matter is not a new way and has been quite successfully applied, including several works of our research group.^{9,10,21,22} However, a controllable variation of the material properties via the SWCNT internal channel filling has not yet been carried out.

Second, we have developed a simple empirical method for prediction and achievement of the required values of the transport and optical characteristics. We propose a simple approach for the macro-objects composed of carbon nanotubes doping characterization. This approach is an empirical representation of the thermoelectric coefficient on the electrical resistance (specific resistance, sheet resistance (R_{sq}), or conductivity) dependence. The relation of the conductivity (σ) and the thermoelectric coefficient (S) is usually used to estimate the mechanism of the charge carrier conductivity. Transport function $\sigma E(E, T)$ determines both σ and S for a certain Fermi level (E_F).²³ Therefore, from the dependence of S versus σ in the course of E_F varying, the charge transport features and $\sigma E(E, T)$ type can be found.²⁴ However, the properties of systems, such as films of carbon nanotubes, depend on a number of parameters: CNT diameters, content of semiconductor and metal fractions, nanotube lengths, number of impurities, number of defects, doping method, orientation of the nanotubes, junctions, etc.^{12,25–28} Therefore, from our point of view, the majority of approximations for determining the main transport characteristics of such objects is rather speculative and often works correctly only for a limited number of specific samples. In our work, we use the $S - R_{sq}/R_{sq-max}$ dependence and propose a general approach, which we call the “doping map”, applicable to all types of macroscopic objects composed of CNTs. This “doping map” gives us complete information about the initial and the doped states of the conducting system. Moreover, the method allows the prediction of the maximum achievable values of transport characteristics at the adjusted doping level (tuned Fermi level). Finally, based on the thermoelectric properties, we demonstrate the achievement of optimal values for parameters required for a specific application task.

2. EXPERIMENTAL DETAILS

2.1. SWCNT Synthesis and Network Preparation. Thin films of SWCNTs for all types of experiments were formed from as-synthesized carbon nanotubes. First, the aerosol chemical vapor deposition (aerosol-CVD) synthesized SWCNTs were used for the formation of conductive thin films.²⁹ These films are networks formed from long bundles of SWCNTs. The nanotubes produced by this method have a mean diameter between 1.8 and 2.0 nm. A typical image of the aerosol SWCNT film is presented in Figure 1 a). The nanotubes arranged in bundles with a diameter of about 100 nm form a network of uniform density. The nanotube network density and thickness are controlled by the accumulation time of SWCNTs on the filter (Millipore, a pore size of about 0.45 μm) during synthesis. As we have shown earlier, the aerosol-CVD synthesized SWCNTs can be efficiently filled with various doping molecules.^{22,30} Moreover, for SWCNTs of large diameter (about 2 nm), the doping is the most effective because of the higher Fermi level shift due to the charge transfer in the SWCNTs with the smallest bandgaps.

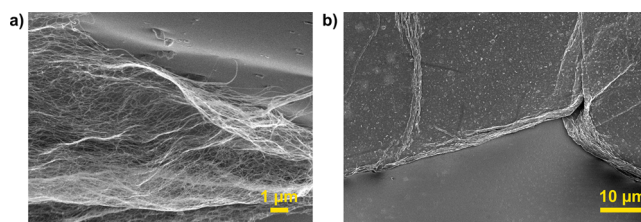


Figure 1. Scanning electron microscopy images of SWCNT films prepared by (a) aerosol chemical vapor deposition and deposited on a filter during synthesis; (b) TUBALL nanotubes separated by the conductivity type. As a second source, we used TUBALL SWCNTs provided by the OCSiAl company (Novosibirsk, Russia).

As with the aerosol-CVD nanotubes, the TUBALL nanotubes have an average diameter of 2 nm. The initial TUBALL powder was suspended in 2% sodium cholate (SC) aqueous solution (in concentration 1 mg of SWCNT powder in 1 mL of solution) and sonicated by the ultrasonic tip Hielscher UP200 (power 200 W) for 4 h in the ice bath. Thereafter, the suspension was ultracentrifuged (Beckman Coulter Ultra-Max-E) at 22 400 g for 1 h, the supernatant was extracted and additionally ultracentrifuged at 360 000 g for 1 h.

Aqueous two-phase polymer extraction technique^{8,31,32} was used to separate SWCNTs by type of conductivity. We used two water-soluble polymers—polyethylene glycol (PEG, 6 kDa, AppliChem) and dextran (Dx, 70 kDa, AppliChem), and two surfactants—sodium cholate (SC, Sigma-Aldrich) and sodium dodecyl sulfate (SDS, AppliChem). The water solutions of polymers and surfactants were prepared in the following concentrations: 20 wt % Dx, 50 wt % PEG, 10 wt % SC, and 10 wt % SDS. The purest semiconducting fraction was achieved with Dx 6.8% w/v, PEG 6.2% w/v, SC 1.3% w/v, SDS 0.6% w/v at 22 °C. The purest metallic fraction was achieved with Dx 6.5% w/v, PEG 5.9% w/v, SC 1.2% w/v, and SDS 0.7% w/v at 22 °C. The final purities of the semiconducting and metallic fractions of TUBALL SWCNTs were 98 and 95%, correspondingly.

For purification of nanotube fractions separated from polymers and surfactants, we added sodium chloride solution and ultracentrifuged the mixtures at 360 000 g for 15 min. Afterward, we used an ultrafiltration cell for dialysis purposes.

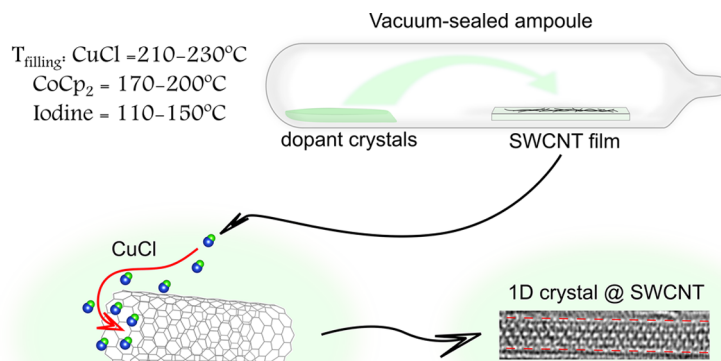
Films of SWCNTs were prepared by vacuum filtration technique with mixed cellulose ester (MCE) membranes with 0.2 μm pores. For optical and electrophysical measurements, strips ((2–3) \times 10 mm) were cut from all types of prepared films. The SWCNT strips were deposited on glass plates and heated at 200 °C in air for 2 h to remove organics. An image of thus prepared film is demonstrated in Figure 1 b). Residual polymers and surfactants can be seen on the surface of these films. However, according to our measurements, it does not significantly affect the doping procedure. To estimate the thickness of these films, we performed atomic force microscopy measurements. The estimated thickness of the films was uniform for every sample and varied between 100 and 250 nm.

2.2. Microscopy. The SWCNT samples imaging has been performed using a scanning electron microscope Zeiss Merlin, Carl Zeiss, Germany. The samples were studied as prepared. Often, the SWCNT films were deposited on Si or glass substrate. Low accelerating voltages were used to minimize the charge accumulation.

In addition to scanning electron microscopy, atomic force microscopy was performed on several samples to measure the thickness on carbon nanotube films. Titanium microscope, NT-MDT, Russia, was used for these measurements. To estimate the thickness of films, we used two approaches. The thickness was measured at the edges and the folds of the films.

2.3. Doping and Annealing Procedure. First, the samples were annealed in a vacuum to remove the adsorbed oxygen and water. Annealing was carried out at temperatures of 100–200 °C either in evacuated ampules or in a stationary evacuated tubular furnace for 12 h. The vacuum level reached was 1×10^{-3} mbar. In the case of ampules, heating was carried out in a standard muffle furnace. The samples were

Scheme 1. Scheme of Filling Procedure of the SWCNT Film; HRTEM Image of SWCNTs Filled with Copper Chloride, and 1D Crystal@SWCNT^a



^aCNT diameter is about 1.5 nm.

then exposed to air with a periodic recording of the transport characteristics of the films.

To fill the SWCNT channels, we applied the gas-phase film processing technique (Scheme 1) that we have successfully used earlier.^{22,30,33} Nanotube networks and dopant crystals (cobaltocene, copper chloride, or iodine) were heated in a sealed tube in an electric furnace. There were no direct contacts between the nanotube network and the dopant. The treatment temperature was close to the sublimation temperature of the dopant materials.

A postfilling procedure includes heating of the filled SWCNT films in air for 2 h under the same treatment conditions but without dopant crystals. This step was performed to partly remove the outer-wall adsorbed dopant crystals.

The internal channels of SWCNTs were filled with cobaltocene ($\text{Co}(\text{C}_5\text{H}_5)_2$, CoCp_2) to obtain the n-doped SWCNT films. The CoCp_2 treatment was carried out at the temperature of about 180 °C³⁴ over 12 h. We used 1–5 mg of solid CoCp_2 (Sigma-Aldrich, powder) for treatment. After filling, the n-doped samples were exposed to air with the periodic recording of the transport characteristics of the film.

The internal channels of SWCNTs were filled with iodine to obtain the softly p-doped SWCNT films. The iodine treatment was carried out in the temperature range of 125–130 °C³³ over 12 h. About 20 mg of solid iodine (Sigma-Aldrich, 99.8%) was used for the treatment process. After the doping procedure, the samples filled with iodine were held in air with periodic measurements of optical and electrophysical properties.

The second p-type dopant used for the same SWCNT films was copper chloride. According to the literature, copper chloride demonstrated a higher, in comparison with iodine, charge transfer value (p-doping).^{35,36} A gas-phase treatment by copper chloride was carried out in the temperature range of 210–230 °C. We used 1–5 mg of solid copper(I) chloride (Alfa Aesar, metals basis, 99.999%) for treatment.

The optical and transport properties of carbon nanotubes were affected by doping.^{36–38} In this work, the doping approach is based on a difference between the WF values of carbon nanotubes ($\sim 4.95\text{--}5.05$ eV^{39,40}) and acceptor material like iodine (~ 5.5 eV⁴¹) and copper chloride ($\sim 6.8\text{--}7.0$ eV⁴²), or donor material such as CoCp_2 (ionization energy ~ 4.0 eV^{43–45}). The electron transfer between the CNT states and the dopant material states depends on their relative energy. In the case of p-doping, the charge transfer results in depletion of the highest occupied nanotube electronic state accompanied by the Fermi level shift inside the valence band of the CNTs,^{10,46} leading to the metallization of the semiconducting fraction of the macroscopic sample. In the case of n-doping, the filling of the lowest unoccupied nanotube electronic state occurs and the Fermi level shifts inside the conduction band. The magnitude of the charge transfer has to depend

both on the WF and the dopant concentration, so these features can be used for doping level control.

For tuning the SWCNT film properties, the method of dopant concentration in the nanotube channels variation was applied. The main parameter for the dopant concentration variation was the time of filling under the same temperature and pressure. We have previously demonstrated a change in optical properties induced by the filling time variation for copper chloride doping.³⁵ The effect of doping in the case of CuCl is several times higher compared to the effect of iodine filling; therefore, we expected a wider range of doping variation in the experiment with CuCl. Thus, we have applied two approaches for CuCl concentration variation in the CNT channels: (1) different treatment time (from 15 min to 26 h) of similar films followed by a comparison of measured transport and optical parameters; (2) a step-by-step filling of the same film (with steps of 15 min or 2 or 4 h) accompanied by measurements of optical and electrophysical parameters of the film between steps.

In this paper, we discuss only optical and transport features that confirm the nanotube filling led to doping. Earlier, we published the HRTEM study^{22,47,48} with direct confirmation of nanotube filling from the gas phase and with the atomic resolution of structure formed inside nanotubes (bottom right image in Scheme 1).

2.4. Optical Measurements of Prepared Materials. The Raman spectra of SWCNT films were obtained with a Jobin Yvon S-3000 spectrometer and an Ar–Kr laser (Spectra-Physics). The Raman spectra of SWNTs were recorded with 532 nm excitation wavelength in the spectral ranges of tangential G-mode (around 1600 cm^{-1}) and radial breathing modes (RBM) (50–500 cm^{-1}).

The UV–vis–NIR optical absorption spectra were recorded within a spectral range of 200–3000 nm with a Lambda-950 spectrophotometer (PerkinElmer).

2.5. Thermoelectric Power (TEP) Measurements. The thermoelectric power (TEP) was measured using an ordinary two-probe method in a specialized vacuum chamber containing a custom-made TEP probe holder. On gradient heating of the holder plate, the sample temperatures and the potential differences across the sample were measured with thermocouples. The chromel–alumel thermocouples were utilized as probes, but the potential differences were measured by alumel wires. The samples of “pristine”, CoCp_2 , and iodine- and copper chloride-filled SWCNT films were held under the ambient conditions before the TEP measurements. The measurements were conducted for a temperature range of 300–425 K (temperature of the hot point of the sample) and in air.

2.6. Four-Probe Measurements of Electrical Sheet Resistance. Measurements of electrical sheet resistance of SWCNT films were performed via a common four-probe resistivity technique on commercially available setup: Jandel RMS-EL/RMS-EL-Z. The

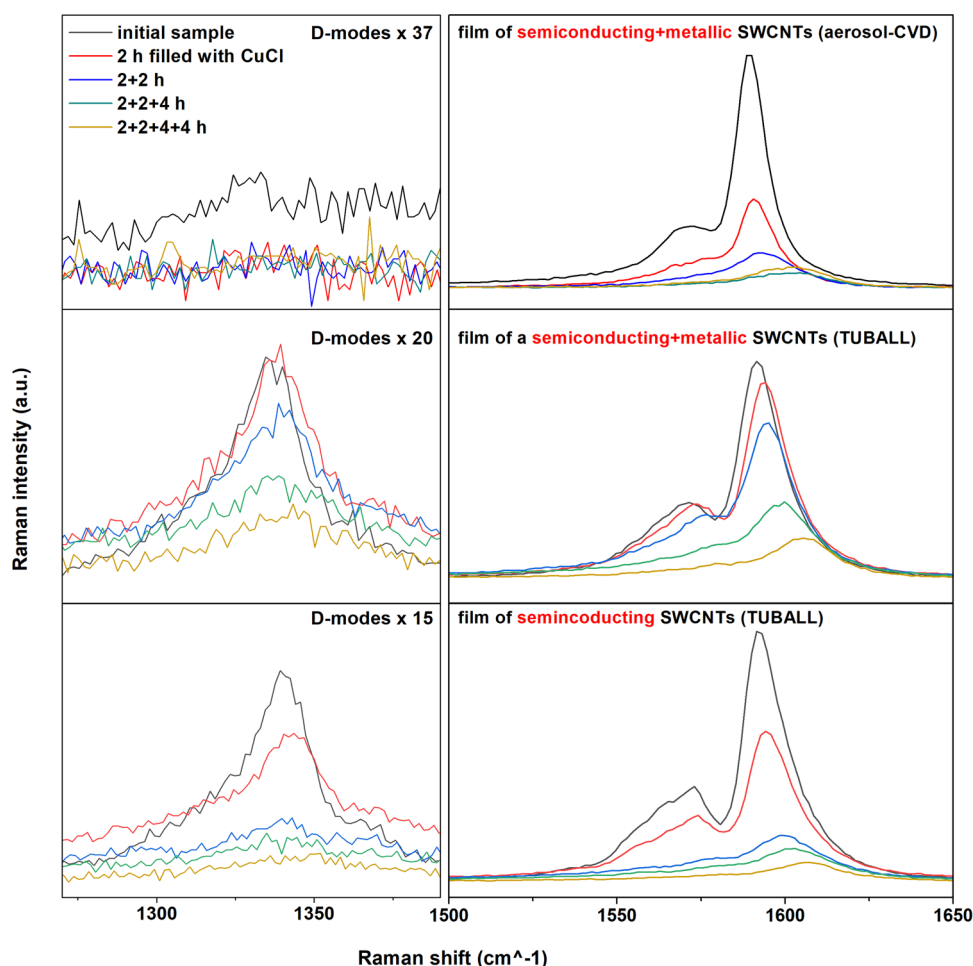


Figure 2. Raman spectra of step-by-step doped SWCNTs with CuCl gas-phase filling process: (1) film of a mixture of semiconductor and metal SWCNTs (aerosol-CVD); (2) film of a mixture of semiconductor and metal SWCNTs (TUBALL); (3) film enriched with semiconductor SWCNTs (TUBALL). The duration of each filling step is 2 h (lines of different colors correspond to the number of doping steps).

measurement range of the setup is from 1 mOhm/sq up to 500 MOhm/sq with a typical accuracy of 0.3%.

2.7. X-ray Photoelectron Spectroscopy and Ultraviolet Photoelectron Spectroscopy. XPS spectra were recorded with a Theta Probe (Thermo Fisher Scientific) using a monochromatic X-ray source Alka with a photon energy of 1486.6 eV. During the survey, the differential charging of the sample was compensated using a low-energy electron beam. To calibrate the binding energy scale, we used the lines Au 4f, Ag 3d, and Cu 2p with a tolerance of ± 0.02 eV. Spectra were recorded in the analyzer constant energy mode. Pass energy during the recording was 100 eV, a step of 0.1 eV, a delay time of 0.1 s, and the number of scans 10. UPS spectra were recorded using UV source with a photon energy of 40.8 eV with negative biasing of the samples (the position of the Fermi edge on the gold sample was -0.02 eV (Boltzmann 80/20)). Pass energy during the recording was 10 eV, a step of 0.05 eV, a delay time of 0.2 s, and the number of scans 10.

3. RESULTS AND DISCUSSION

3.1. Raman Measurements. The most convenient and widely used method for the qualitative characterization of the doping level of carbon nanotubes is Raman spectroscopy. Under doping due to the strong electron–phonon interaction, a softening of the phonon modes of CNTs is observed according to the Kohn anomaly for the CNT LO modes.^{49,50} In the Raman spectra, the effect is manifested in the shift of CNT G-mode. It was shown earlier that the magnitude of the G-mode shift is related to the amount of charge transfer.^{37,51} The magnitude of

the G-mode shift can be related both to the efficiency (WF difference) of the dopants and their concentration in the nanotube sample. In the Raman spectra, we previously observed a difference in G-mode shifts for nanotubes depending on the dopant type and treatment time.^{22,35}

Figure 2 shows the step-by-step treatment of similar films with copper chloride (each step of the treatment was performed for at least 2 h at the temperature of 230 °C) leading to a smooth shift of the G-mode position and peak intensity decrease for all types of nanotubes. Under the step-by-step treatment, the G-mode was shifted from 1590 cm^{-1} (for as-prepared films) to 1608 cm^{-1} (for the saturated doping). The absence of the D-mode intensity growth indicates the absence of oxidative and destructive effects. The equal changes are observed both in the step-by-step treatment of one film and in the case of similar films with different treatment times.³⁵

Doping with iodine also leads to a resolved shift of the G-mode. However, the effect is much weaker. In the case of saturated doping with iodine (13 h treatment), the G-mode shift does not exceed the case of a short-term filling with copper chloride (2–4 h of treatment).²² As expected in the case of iodine doping, the change of processing time does not result in repeatable and stable doping. In case of doping with CoCp_2 (see Supporting Information), no significant shifts of G-mode parameters are observed in Raman spectra, which is associated with a weak doping effect.^{43,45}

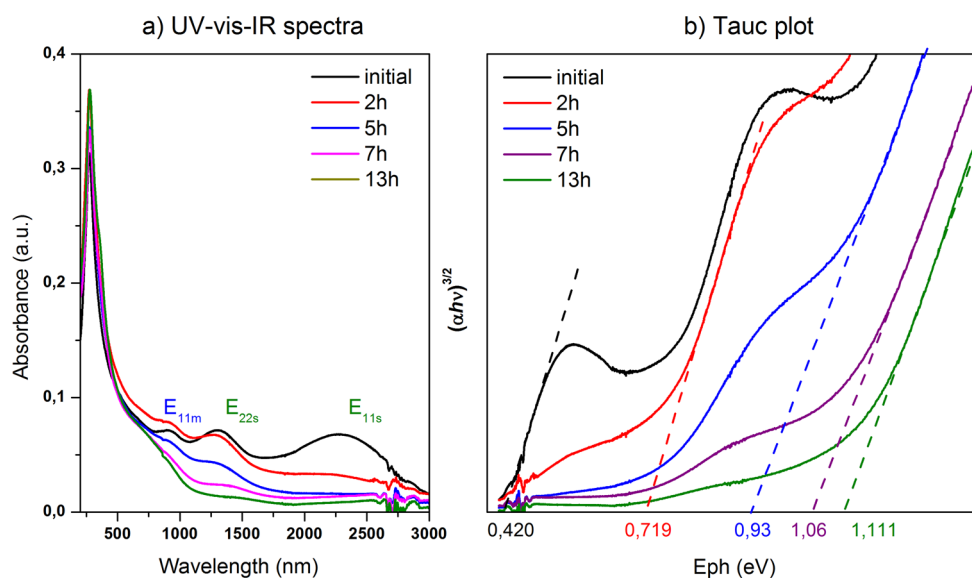


Figure 3. (a) UV–vis–NIR absorbance spectra of step-by-step doped SWCNTs with CuCl gas-phase filling process; (b) Tauc and Davis–Mott plots: $(\alpha h\nu)^{3/2}$ as a function of $E_{ph} = (h\nu - E_g)$.

3.2. Optical Absorption Measurements. UV–vis–NIR spectroscopy is a standard method for visualizing the doping of single-walled carbon nanotube macrosystems. In the UV–vis–NIR spectra, suppression of the absorption bands (E_{11s} , E_{22s} , or E_{11m}) is the main effect of the doping process (Figure 3a). Suppression of the optical absorption bands of nanotubes is a consequence of the Burstein–Moss shift,^{52,53} usually observed in degenerate semiconductors. For the SWCNTs, this significantly affects the optical properties of the samples.^{15,33,54} As in the case of Raman scattering, both methods for varying the impurity concentration (step-by-step doping or different times of exposure to copper chloride) lead to a gradual shift in the Fermi level position, which is manifested in the gradual suppression of the absorption spectra (Figure 3a). Similar effects are observed when dopants with different concentrations are deposited on the surface of CNTs.¹⁴ To estimate the change in the optical band gap edge (E_g) due to the tunable doping, the Tauc and Davis–Mott relations were used: $(\alpha h\nu)^n$ as a function of $(h\nu - E_g)$ calculated from UV–vis–IR absorbance coefficient (α) data of CuCl@SWCNT films. The edge of optical energy gap is estimated by extrapolation of the linear dependence which occurs generally in the absorption data,⁵⁷ as shown in Figure 3b). We use the Tauc relation given by

$$(\alpha h\nu)^n = (h\nu - E_g) \quad (1)$$

In our case, the index n is 3/2 in eq 1. The procedure for selection of the index n for the optical band gap evaluation is described in detail in the Supporting Information. Calculations show that for the studied samples, the step-by-step doping with copper chloride (p-dopant) leads to the optical gap edge (E_g) shifting from 0.42 eV (nondoped CNTs) to 1.11 eV (efficiently doped nanotubes) (Figure 3b).

3.3. XPS and UPS Measurements. To confirm the gradual increase in dopant concentration with the processing time both in the stepwise and continuous processes, which we consider the main parameter for tuning the doping parameter, the XPS method was used. In Figure 4, the XPS-spectra of Cu 2p for nanotubes with different processing times by filling with copper chloride(I) are presented. Both CuCl and CuCl₂ were observed for all doped samples but in different ratios. The content of

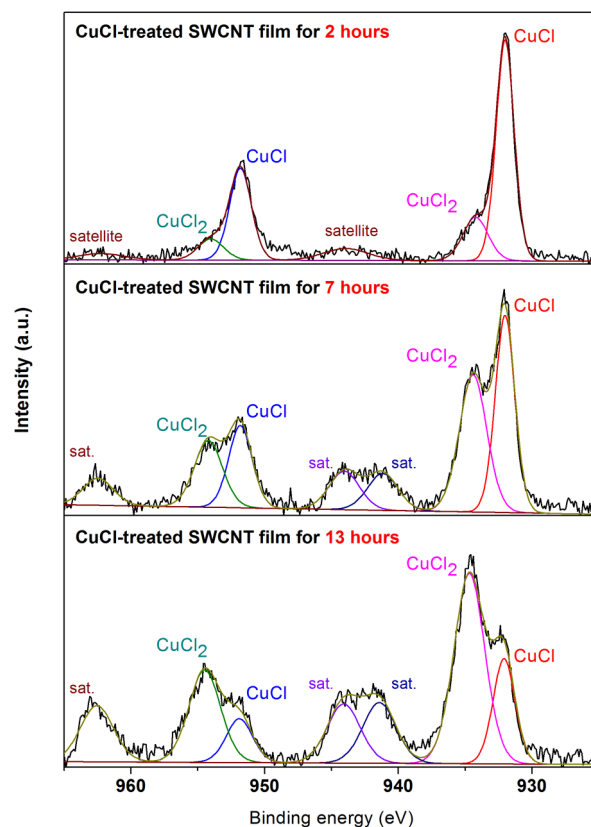
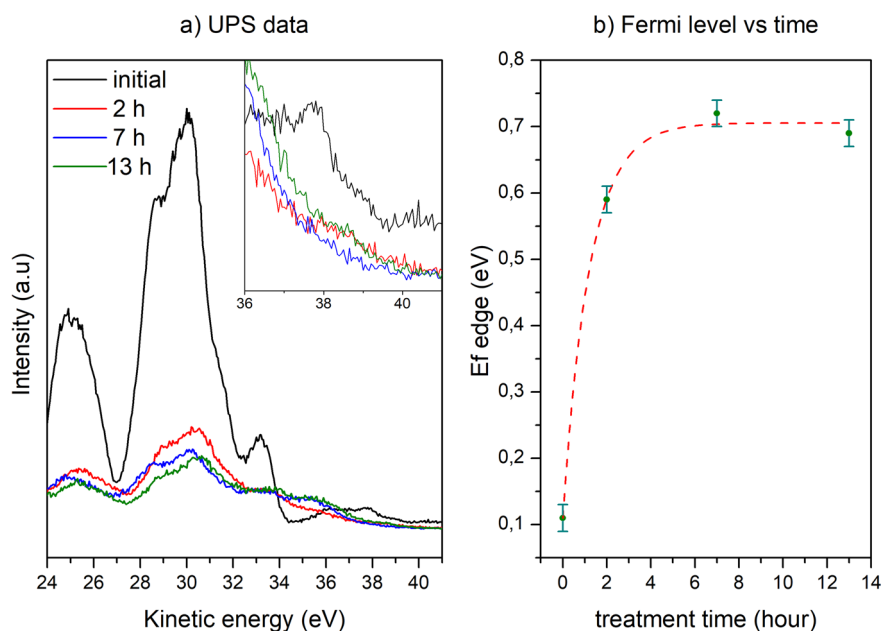


Figure 4. X-ray photoelectron spectra (Cu 2p region) for CuCl-treated SWCNT film for 2, 7, and 13 h.

CuCl₂ increases with the treatment time as indicated by an increase in the characteristic satellite intensity. The reason for this may be the disproportionation reaction of copper chloride, $2\text{CuCl} \rightarrow \text{Cu} + \text{CuCl}_2$,⁵⁹ under temperatures above 100 °C, which corresponds to the filling conditions for SWCNTs. To estimate the content of copper chlorides in our samples, we fitted the spectra using the reference data for CuCl (932 eV⁶⁰) and CuCl₂ (934.7 eV⁶¹). During decomposition, the Cu 2p_{1/2}

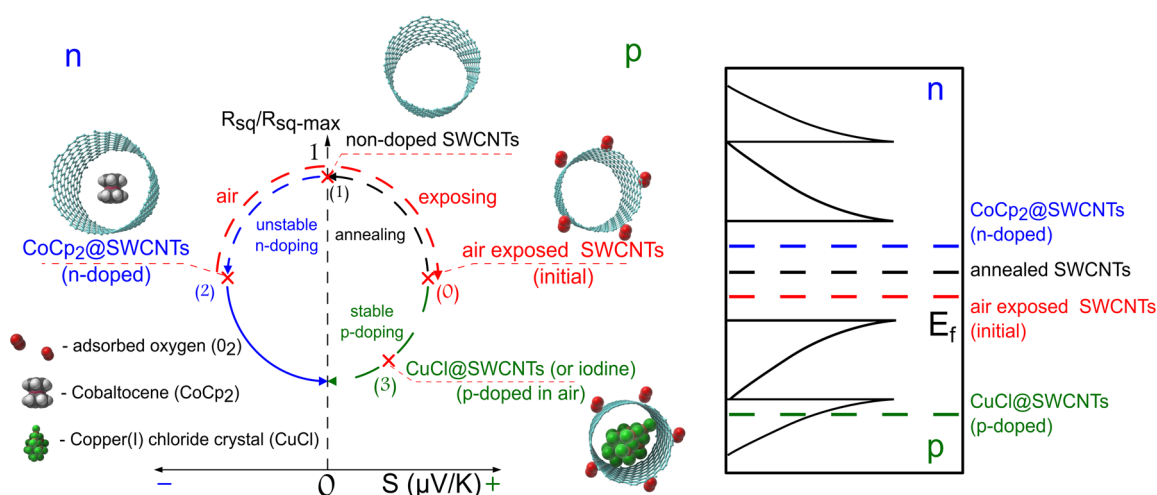
Table 1. Fitted Parameters of Cu 2p_{3/2} Components Depending on the Treatment Time, Ratio of Copper Chloride 2+ to 1+, and Total Copper Content in the Samples

doping time (h)	CuCl			CuCl ₂			CuCl ₂ /CuCl ration (a.u.)	Cu content (at. %)
	position (eV)	fwhm	area (%)	position (eV)	fwhm	area (%)		
2	932.01	1.59	78.05	934.24	2.22	21.95	0.28	2.25
7	932.02	1.75	50.37	934.43	2.46	49.63	0.99	3.51
13	932.10	1.93	28.34	934.68	2.70	71.66	2.53	3.75

**Figure 5.** Valence band spectra near the Fermi energy level for initial (black line), for CuCl-treated SWCNT film for 2 (blue line), 7 (orange line), and 13 (green line) h. (a) UPS data; (b) Fermi level position versus treatment time.

Model Doping Map for CNT

DoS

**Figure 6.** Model “doping map” based on experimental cycle for characterization of SWCNT macro-objects. The key points of $S-R_{sq}/R_{sq-max}$ dependence of the macro-object system containing SWCNTs: (0) a stable state in the air - “initial” films; (1) not stable in air, undoped sample (annealed); (2) not stable in air n-doped sample; (3) stable in air p-doped sample. The dashed lines on the graph show the experimental stages carried out to plot the dependence: the black line is the annealing of the initial sample, the transition from point (0) to (1); the blue line is the n-doping of the initial sample, the transition from point (0) to (2); the green line is the p-doping of the initial sample, the transition from point (0) to (3); the red line is exposing of n-doped or annealed samples to air to plot intermediate dependence points (between (2) and (0) or (1) and (0), respectively). Density of states (DoS) diagram of CNT for the experiments performed. The “doping map” is based on the relation of the thermopower coefficient (x -axis) versus R_{sq}/R_{sq-max} (R_{sq} sheet resistance, y -axis). The (R_{sq}/R_{sq-max})-axis is a logarithmic scale (log scale).

Empirical Doping Map

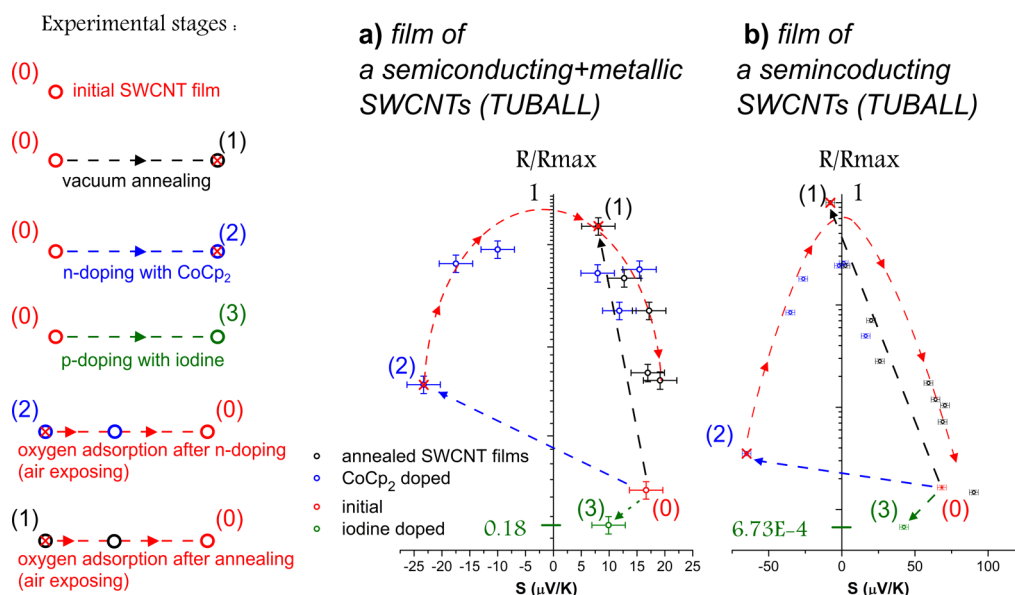


Figure 7. (a) Empirical “doping map” for the film of mixed SWCNTs (TUBALL) and (b) film enriched with semiconductor SWCNTs (TUBALL). The “doping map” is based on the relation of the thermopower coefficient versus $R_{\text{sq}}/R_{\text{sq-max}}$ (R_{sq} , sheet resistance). The ($R_{\text{sq}}/R_{\text{sq-max}}$)-axis is a logarithmic scale (log scale).

components were involved. Satellites were approximated by fixed Gaussians. The change in position of the Cu $2p_{3/2}$ components is shown in Table 1.

The peak position of CuCl practically does not change, whereas under the short processing times, the CuCl_2 is in an unusual position. This may be due to the presence of insignificant amounts of copper 1+, which according to ref 62 can lead to similar changes in the peak position toward the lower binding energies. This may also be due to the influence of organofluorine compounds, which are artifacts of plasma-chemical etching of silicon.

The data from Table 1 show the dependence of the change in the ratio of CuCl_2 to CuCl and the total copper content with increasing processing time from 2 to 13 h. According to Table 1 data, we expect similar behavior of the Fermi level position shift. On the basis of UPS data (Figure 5a), we obtain a strongly logarithmic curve of the Fermi level position depending on the processing time (Figure 5b). The Fermi level position was determined by the linear approximation. The difference in the basic value of the Fermi level can be explained by the initial presence of oxygen in the starting material (oxygen atoms on the defects).

3.4. Thermopower Measurements. On the basis of previous studies of the nanotube film doping and the fundamental dependence of the Seebeck coefficient on conductivity, an approach was proposed for SWCNT macrosystems calibrating and characterizing.^{14,22,63,64} The method is based on a simple empirical reconstruction representation of the dependence of the intrinsic thermoelectric power coefficient (S) versus the ratio of the sheet resistance (or specific conductivity of the films) to the maximum possible sheet resistance of the studied macrosystem ($R_{\text{sq}}/R_{\text{sq-max}}$). Each point of the reproduced “doping map” corresponds to the state of the same macro-object with different positions of Fermi level. In our experiment, the Fermi level position is tuned by adjusting the dopant concentration in the CNT channels or by adjusting adsorption and desorption of oxygen on the CNT surface.

The diagram in Figure 6 shows the form of $S-R_{\text{sq}}/R_{\text{sq-max}}$ dependence and the method of its plotting using the example of our experimental cycles. On the “doping map”, the four key points of the system can be noted: (0) a stable state in the air—weak doping with oxygen (physically and chemically adsorbed)—usually called as “initial” or “as-prepared” films; (1) a point with the maximum resistance is the nondoped state that can be achieved by complete cleaning (annealing) or reduction of the oxidized sample; (2) not stable in air n-doped state, which is achieved by doping with frequently used organic and inorganic n-dopants; (3) stable in air p-doped state, for example, doping with iodine or CuCl. These key points conditionally divide the dependence into four segments: (0)–(1), a weak and unstable p-doping with physically and chemically adsorbed oxygen; (1)–(2), a weak and unstable n-doping in the air; (0)–(3), a stable and tunable p-doping region; region below point (2), n-doping region. In our study, only the first three segments of the “doping map” are considered, as they are experimentally reproducible and easily achievable. The (0)–(1) segment is plotted by periodically measuring the S and R_{sq} values of the initial SWCNT film after annealing procedure during the oxygen adsorption. The (1)–(2) segment is plotted by periodically measuring the S and R_{sq} values of the SWCNT film after the n-doping procedure during oxygen adsorption. This is primarily due to p-doping, which occurs due to the physical adsorption of oxygen from the environment. Obviously, the studied system - $\text{CoCp}_2/\text{CNT}/\text{O}_2$ after charge transfer occurs, has a common Fermi level. The position of the Fermi level of this system, or the type of doping, will be determined by the HOMO–LUMO of molecules and WF of the SWCNT. In our case, p-doping with oxygen compensates for n-doping from CoCp_2 . Thus, these segments of the dependence are unstable in the air. In contrast, the (0)–(3) segment can be fully reproduced using the controlled p-doping, for example, tunable doping with CuCl. We consider the oxygen effect for an acceptor filled-SWCNT film negligible due to a strong doping and a significant Fermi level shift for this region.²²

Empirical Doping Map for p-doping

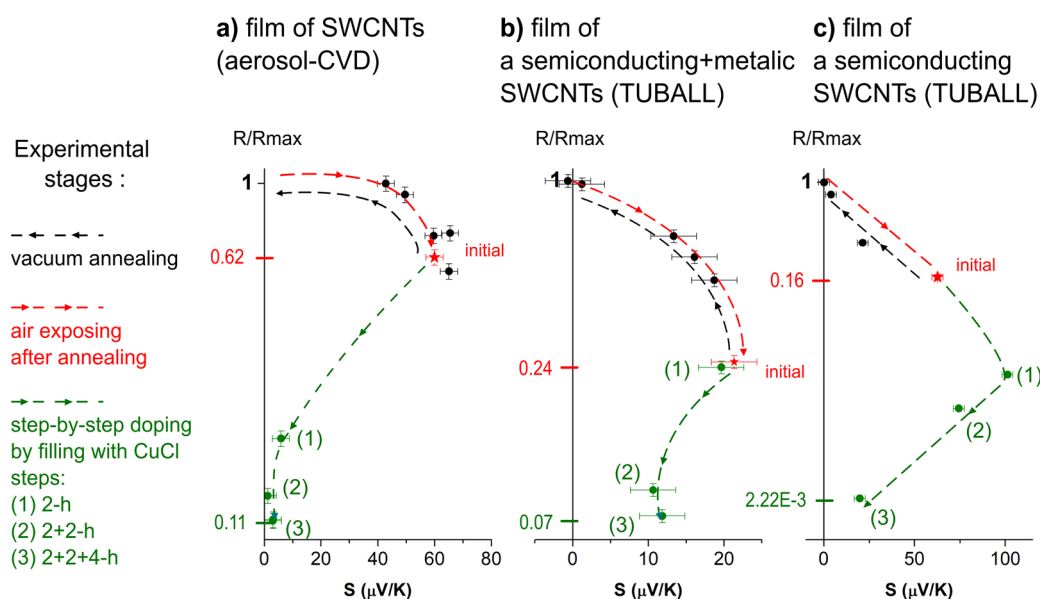


Figure 8. “Doping map” of doped with CuCl SWCNT film: (a) film of mixed SWCNTs (aerosol-CVD); (b) film of mixed SWCNTs (TUBALL); (c) film enriched with semiconductor SWCNTs (TUBALL). The films are filled with CuCl by the step-by-step treatment method: (1) 2 h treatment, (2) 2 h treatment, (3) 4 h treatment. The (R_{sq}/R_{sq-max}) -axis is a logarithmic scale (log scale).

The form of the $S-R_{sq}/R_{sq-max}$ curve (as well as $S-\sigma$) is primarily determined by the SWCNT density of states.^{27,65} S according to the Mott formula for degenerate semiconductors is represented

$$S = (\pi^2)(k_B^2) \left(\frac{T}{3q} \right) \left(\frac{d \ln \sigma(E)}{dE} \right) \Big|_{E = E_F} \quad (2)$$

S , according to the Boltzmann equations for nondegenerate semiconductors, has the form

$$S = \left(\frac{k_B}{q} \right) \left[\frac{(E - E_F)}{k_B T} \right] \quad (3)$$

where k_B is the Boltzmann constant, q is the charge, T is the temperature, and E is the electron energy.^{66,67} The sign of the region at the “doping map” is determined by the type of charge carriers (q in formula 2 and 3). The shape of the “doping map” and values are determined by the diameters and type of carbon nanotubes. The position of the key points on the “doping map” is determined by two parameters: diameter and Fermi level shift upon doping with oxygen, which is higher for nanotubes with a smaller bandgap (larger diameters, respectively).

Figure 7a, b shows the experimentally obtained “doping map” of the following samples: (1) film containing a mixture of semiconductor and metal SWCNTs; (2) film enriched with semiconductor SWCNTs. A simple way to reconstruct a low p-doping area of the “doping map” is annealing in a vacuum to remove adsorbed oxygen and water (on Figure 7 is (0)–(1) region). The sheet resistance and thermoelectric coefficient must be measured in the air until providing almost complete restoration of the initial parameters. In Figure 7a, b, point (1) is the state of the system after annealing at the moment of the ampule opening. The subsequent black dots show the adsorption of oxygen from the air. After exposing in the air for 2 days and transport characteristics recovery, this film was filled with CoCp₂ to achieve a weak n-doping–point (2). The sheet

resistance and the Seebeck coefficient were measured daily in the air for 7 days from the moment the vacuum ampule was opened (point (2) on Figure 7) until the initial parameters were almost completely restored. The states of the samples inside the region of weak n- and p-doping ((2)–(0) on Figures 6 and 7) are poorly detectable in optical absorption and practically do not lead to changes in Raman scattering (according to the Kohn anomaly for the CNT LO modes⁵⁰). This region is characterized by the weak charge transfer from oxygen molecules (depending on the diameter, it can reach 0.1 electron from the carbon nanotube to every oxygen molecule⁶⁸). In the case of n-doping, a low charge transfer is due to the small difference between the HOMO for CoCp₂ (ionization energy 4.0 eV⁶⁹) and the bottom of the conduction band for SWCNTs (WF about 4.9 eV). According to the “doping map”, the magnitude of the charge transfer level at the CoCp₂ filling is comparable to that of doping with oxygen from the environment (Figure 6). As in the case of p-doping with environmental oxygen, for n-doping with CoCp₂, there are no significant changes in the Raman spectra of SWCNTs (see Supporting Information). However, for transport characteristics (R_{sq} or S), the weak-doping areas ((2)–(0) on Figures 6 and 7) are strongly sensitive to charge transfer.

The region of stable p-doping ((0)–(3)) is presented in Figure 7a, b. The method of gas-phase filling of CNTs with iodine in vacuum ampules was used. We have demonstrated earlier²² that the sample parameters do not change with time under oxygen adsorption. For iodine-filled SWCNTs with a small diameter, the electric charge transfer is up to 0.3 electron per iodine atom (depending on the iodine structure). The Fermi level shift is up to 0.23 eV below the top of the nanotube valence band.⁷⁰ The drop in electrical resistance under iodine doping does not exceed an order of magnitude, compared to the area of weak oxygen doping ((1)–(0) on Figures 6 and 7).^{22,30}

The resulting “doping map”, in general, has the shape of an elliptic curve (which is due to $S(E)$ dependence). The “intersection” of the curve with the y -axis ($R_{sq}/R_{sq-max} = 1$)

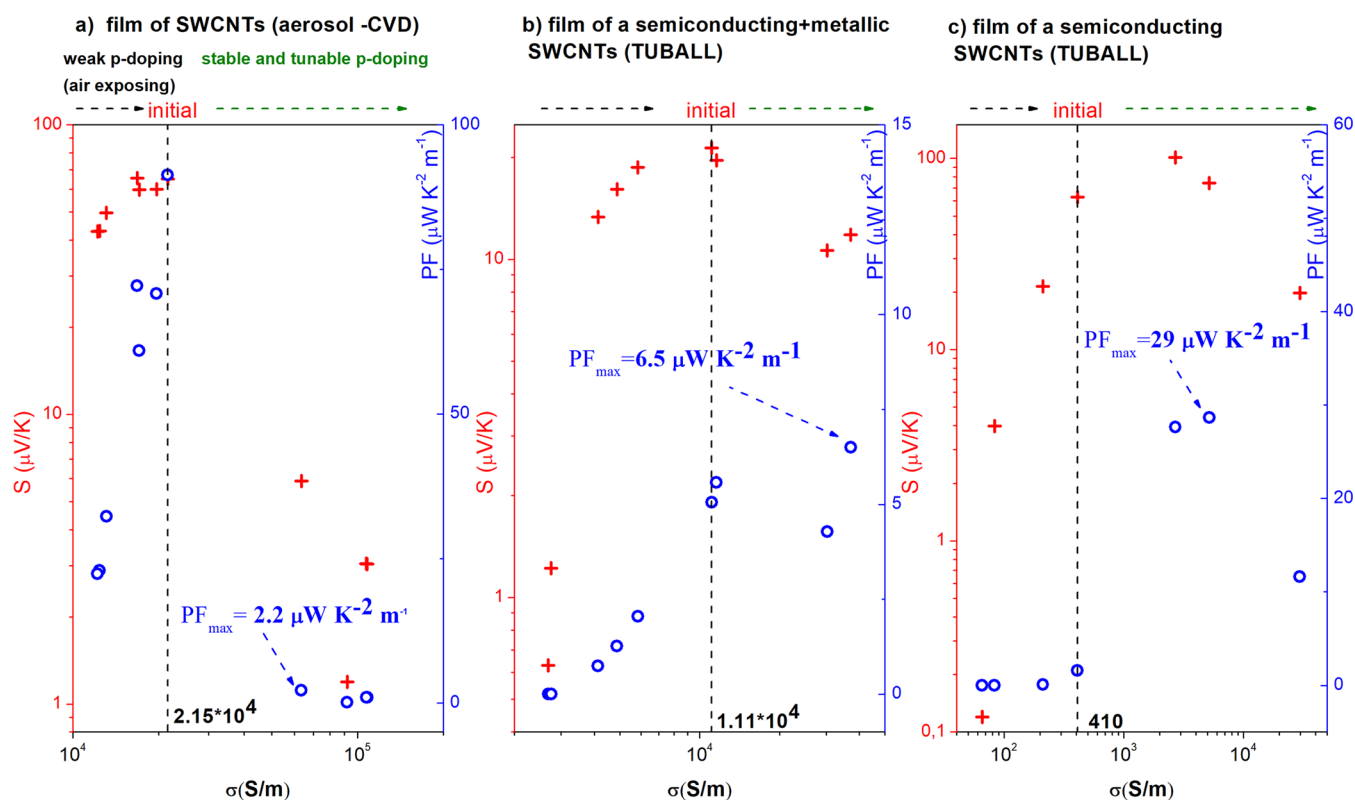


Figure 9. Effect of tunable doping of SWCNT films with CuCl on the thermopower coefficient (S)–electrical conductivity (σ) relation (red crosses). The effect of tunable doping of SWCNT films with CuCl on the power factor (PF)–electrical conductivity (σ) relation (blue circles) for (a) film of mixed SWCNTs (aerosol-CVD); (b) film of mixed SWCNTs (TUBALL); (c) film enriched with semiconductor SWCNTs (TUBALL). The figures show the maximum power factor (PF_{\max}) values stable in time.

corresponds to the annealed film with the highest possible resistance and the lowest thermoelectric coefficient (E_f in the center of the semiconductor nanotube bandgap). As follows from the presented experimental results, to complete the mapping of macrosystem properties in the region of weak n- and p-doping, the vacuum annealing is sufficient. This is due to the symmetrical form of almost elliptic dependence (in log scale) of $S-R_{\text{sq}}/R_{\text{sq-max}}$. The shape varies depending on the composition and morphology of the film. A discrepancy from the elliptic shape is manifested for films with pronounced metallicity Figure 7a and enriched with semiconducting nanotubes as shown in Figure 7b.

We have applied the “doping map” method to justify of p-doping with CuCl of SWCNT macro-objects in the air environment. The concentration of copper chloride in the internal channels of SWCNTs was controllably varied. Figure 7 shows the “doping map” ($S-(R_{\text{sq}}/R_{\text{sq-max}})$) for nanotubes with a narrow diameter distribution (mean diameter about 2 nm), aerosol-CVD, and TUBALL-type nanotubes. Films of semiconducting+metallic nanotubes and sorted semiconducting nanotubes were prepared from Tuball-type nanotubes. As in the previous samples, the films were annealed in a vacuum (black arrow in Figure 8) and exposed in air (red arrow in Figure 8) for the reproduction of an unstable p-doping region. Then these films were doped with copper chloride in ampules in a step-like manner (green arrow in Figure 8): (1) 2 h treatment; (2) 2 + 2 h treatment; (3) 2 + 2 + 4 h treatment. The measurements of transport characteristics were carried out after each treatment stage. The p-doping area of the “doping map” is characterized by a smooth change in transport properties converging to an asymptotic value correlated with the doping saturation observed

in XPS and UPS measurements. The p-doping region is characterized by high stability of doping, which is primarily associated with the high Fermi level shift (according to the UPS, the shift value changes from 0.1 to 0.7 eV, and according to the Tauc graph, the change in the optical edge is about 0.7 eV). In our earlier work,³⁶ the maximum value of the Fermi level shift was 0.9 eV for films composed of aerosol nanotubes doped with copper chloride. Thus, the variation of copper chloride concentration in the films presented in this work allows tuning the position of Fermi level from 0.1 to 0.9 eV.

To demonstrate the convenience of the proposed method, we vary the parameters necessary for the production of effective thermopower-based devices. Figure 9 shows the S – σ and power factor (PF)– σ dependencies for three films described in the “doping map” (Figure 7), where power factor is the $PF = (S^2)\sigma$. The plot in Figure 8 can be conditionally divided into two areas relative to the point of the initial sample (stable in the air under ambient $T = 300$ K): the region of unstable p-doping with oxygen and the region of tunable p-doping with CuCl. According to the experimentally obtained data p-doping with oxygen, depending on the CNT type and morphology of the film allows to achieve the highest values ($S \approx 100 \mu\text{V/K}$ and $PF \approx 100 \mu\text{W}/(\text{m K}^2)$) of the coefficient of thermoelectric power and/or PF. However, without additional protection against oxygen adsorption (desorption), these characteristics cannot be stabilized. The initial state (as-prepared sample), which in some cases demonstrates the highest values of thermoelectric parameters, are not stable at temperatures exceeding the room temperature.²² In the region of stable p-doping, the optimum PF value is observed for these films, which is achieved with the CuCl doping (at 2 h treatment). This doping is stable for several years,

and therefore the parameters of conductivity and thermopower remain static, even at elevated up to 100–150 °C temperatures. These films do not require additional lamination procedures. Thus, the developed tunable doping procedure makes it possible to produce macro-objects with the specified transport and optical characteristics that are stable in air.

CONCLUSION

In this work, we present a method for controllable variation of optical and electrophysical parameters of macroscopic objects composed of SWCNTs. The main feature of this tunable doping is the change in the dopant concentration in SWCNT channels by varying the duration of the gaseous filling procedure. We demonstrate that doping with copper chloride allows the variation of the Fermi level position in the range from 0.1 to 0.9 eV and optical absorption edge from 0.42 to 1.11 eV. Also, in this work, we propose a general approach for calibrating, analyzing, and characterizing SWCNT conductive macrosystems and similar structures. The approach is based on the empirical compiling of the $S-R_{sq}/R_{sq-max}$ dependence. We have shown that a simple vacuum annealing experiment can help to map and estimate the transport characteristics of SWCNT macro-objects. Measurement of thermoelectric power between iterations of SWCNTs step-stage-filling made it possible to register and to describe the properties of weakly doped SWCNTs. The “doping map” method allows the complete evaluation of the SWCNT macro-object capabilities for production of effective electronic components. The tunable p-doping method based on SWCNTs filling presented here provides the achievement and conservation of the maximum possible values of power factor and thermoelectric power coefficient for investigated films. We believe that the tuning method developed in this work for optical and electrophysical properties of nanotube networks adjustment is promising for the production of elements with a given WF, transport characteristics, and optical gap.

ASSOCIATED CONTENT

Supporting Information

The Supporting Information is available free of charge at <https://pubs.acs.org/doi/10.1021/acsnm.1c00411>.

Figure S1, normalized Raman spectra of CoCp₂ filled SWCNTs; Figure S2, Kataura plot segment for semiconducting SWCNTs; Figure S3, UV–vis–NIR absorption spectra of initial SWCNT suspension, the semiconducting fraction, and the metallic fraction after the aqueous two-phase extraction procedure; Figure S4, UV–vis–NIR absorbance spectra of SWCNT film on sodalime glass substrate; Figure S5, UV–vis–NIR spectra of films of semiconducting+metallic and semiconducting SWCNTs (TUBALL); Figure S6, sheet resistance versus time of filling with copper chloride (PDF)

AUTHOR INFORMATION

Corresponding Author

Alexander A. Tonkikh – A.M. Prokhorov General Physics Institute, Russian Academy of Science, 119991 Moscow, Russia; Moscow Institute of Physics and Technology, Dolgoprudny 141701, Moscow Region, Russia; orcid.org/0000-0003-0053-3619; Email: aatonkikh@gmail.com

Authors

Valentina A. Eremina – A.M. Prokhorov General Physics Institute, Russian Academy of Science, 119991 Moscow, Russia; Moscow Institute of Physics and Technology, Dolgoprudny 141701, Moscow Region, Russia; orcid.org/0000-0003-0878-0198

Ekaterina A. Obraztsova – A.M. Prokhorov General Physics Institute, Russian Academy of Science, 119991 Moscow, Russia; Shemyakin-Ovchinnikov Institute of Bioorganic Chemistry of the Russian Academy of Sciences, Moscow 117997, Russia; orcid.org/0000-0002-0086-0970

Dmitry A. Musatov – A.M. Prokhorov General Physics Institute, Russian Academy of Science, 119991 Moscow, Russia; Moscow Institute of Physics and Technology, Dolgoprudny 141701, Moscow Region, Russia; orcid.org/0000-0002-2163-3822

Alexander Yu. Pereyaslavtsev – Dukhov Automatics Research Institute (VNIIA), Moscow 127055, Russia; orcid.org/0000-0001-6983-7077

Esko I. Kauppinen – Department of Applied Physics, School of Science, Aalto University, Espoo FI-00076, Finland; orcid.org/0000-0003-1727-8810

Elena D. Obraztsova – A.M. Prokhorov General Physics Institute, Russian Academy of Science, 119991 Moscow, Russia; Moscow Institute of Physics and Technology, Dolgoprudny 141701, Moscow Region, Russia; orcid.org/0000-0003-3001-2996

Complete contact information is available at: <https://pubs.acs.org/10.1021/acsnm.1c00411>

Author Contributions

The manuscript was written through contributions of all authors. All authors have given approval to the final version of the manuscript. All authors contributed equally.

Notes

The authors declare no competing financial interest.

ACKNOWLEDGMENTS

The reported study was funded by RFBR and Moscow city Government according to the research project 19-32-70004. The Raman studies were funded by RSF project 20-42-08004. The separation of SWCNTs by type of conductivity were funded by RFBR project 18-32-00998. The reported study was funded by RFBR, project 20-32-70013.

REFERENCES

- (1) Javey, A.; Guo, J.; Wang, Q.; Lundstrom, M.; Dai, H. Ballistic Carbon Nanotube Field-Effect Transistors. *Nature* **2003**, *424* (6949), 654–657.
- (2) Kataura, H.; Kumazawa, Y.; Maniwa, Y.; Umezumi, I.; Suzuki, S.; Ohtsuka, Y.; Achiba, Y. Optical Properties of Single-Wall Carbon Nanotubes. *Synth. Met.* **1999**, *103* (1–3), 2555–2558.
- (3) Shi, J.; Chu, H.; Li, Y.; Zhang, X.; Pan, H.; Li, D. Synthesis and Nonlinear Optical Properties of Semiconducting Single-Walled Carbon Nanotubes at 1 Mm. *Nanoscale* **2019**, *11* (15), 7287–7292.
- (4) Chu, H.; Li, Y.; Wang, C.; Zhang, H.; Li, D. Recent Investigations on Nonlinear Absorption Properties of Carbon Nanotubes. *Nanophotonics* **2020**, *9* (4), 761–781.
- (5) Xiang, L.; Xia, F.; Jin, W.; Zeng, X.; Liu, F.; Liang, X.; Hu, Y. Carbon Nanotube Dual-Material Gate Devices for Flexible Configurable Multifunctional Electronics. *Carbon* **2020**, *161*, 656–664.
- (6) Xing, Z.; Zhao, J.; Shao, L.; Xiao, H.; Liu, T.; Cui, Z. Highly Flexible Printed Carbon Nanotube Thin Film Transistors Using Cross-Linked Poly(4-Vinylphenol) as the Gate Dielectric and Application for

- Photosensitive Light-Emitting Diode Circuit. *Carbon* **2018**, *133*, 390–397.
- (7) Dai, H.; Thostenson, E. T. Scalable and Multifunctional Carbon Nanotube-Based Textile as Distributed Sensors for Flow and Cure Monitoring. *Carbon* **2020**, *164*, 28–41.
- (8) Khripin, C. Y.; Fagan, J. A.; Zheng, M. Spontaneous Partition of Carbon Nanotubes in Polymer-Modified Aqueous Phases. *J. Am. Chem. Soc.* **2013**, *135* (18), 6822–6825.
- (9) Tonkikh, A. A.; Rybkovskiy, D. V.; Orekhov, A. S.; Chernov, A. I.; Khomich, A. A.; Ewels, C. P.; Kauppinen, E. I.; Rochal, S. B.; Chuvilin, A. L.; Obraztsova, E. D. Optical Properties and Charge Transfer Effects in Single-Walled Carbon Nanotubes Filled with Functionalized Adamantane Molecules. *Carbon* **2016**, *109*, 87–97.
- (10) Eliseev, A.; Yashina, L.; Kharlamova, M.; Kiselev, N. One-Dimensional Crystals inside Single-Walled Carbon Nanotubes: Growth, Structure and Electronic Properties. In *Electronic Properties of Carbon Nanotubes*; InTech: Rijeka, Croatia, 2011.
- (11) Mallakpour, S.; Soltanian, S. Surface Functionalization of Carbon Nanotubes: Fabrication and Applications. *RSC Adv.* **2016**, *6* (111), 109916–109935.
- (12) Piao, M.; Joo, M.-K.; Na, J.; Kim, Y.-J.; Mouis, M.; Ghibaudo, G.; Roth, S.; Kim, W.-Y.; Jang, H.-K.; Kennedy, G. P.; Dettlaff-Weglikowska, U.; Kim, G.-T. Effect of Intertube Junctions on the Thermoelectric Power of Monodispersed Single Walled Carbon Nanotube Networks. *J. Phys. Chem. C* **2014**, *118* (46), 26454–26461.
- (13) Zhang, S.; Nguyen, N.; Leonhardt, B.; Jolowsky, C.; Hao, A.; Park, J. G.; Liang, R. Carbon-Nanotube-Based Electrical Conductors: Fabrication, Optimization, and Applications. *Adv. Electron. Mater.* **2019**, *5* (6), 1800811.
- (14) Avery, A. D.; Zhou, B. H.; Lee, J.; Lee, E.-S.; Miller, E. M.; Ihly, R.; Wesenberg, D.; Mistry, K. S.; Guillot, S. L.; Zink, B. L.; Kim, Y.-H.; Blackburn, J. L.; Ferguson, A. J. Tailored Semiconducting Carbon Nanotube Networks with Enhanced Thermoelectric Properties. *Nat. Energy* **2016**, *1* (4), 16033.
- (15) Kopylova, D. S.; Satco, D. A.; Khabushev, E. M.; Bubis, A. V.; Krasnikov, D. V.; Kallio, T.; Nasibulin, A. G. Electrochemical Enhancement of Optoelectronic Performance of Transparent and Conducting Single-Walled Carbon Nanotube Films. *Carbon* **2020**, *167*, 244–248.
- (16) Tsapenko, A. P.; Romanov, S. A.; Satco, D. A.; Krasnikov, D. V.; Rajanna, P. M.; Danilov, M.; Volobueva, O.; Anisimov, A. S.; Goldt, A. E.; Nasibulin, A. G. Aerosol-Assisted Fine-Tuning of Optoelectrical Properties of SWCNT Films. *J. Phys. Chem. Lett.* **2019**, *10* (14), 3961–3965.
- (17) Zhukov, A. A.; Chernysheva, M. V.; Eliseev, A. A. Measurements of the Work Function of Single-Walled Carbon Nanotubes Encapsulated by AgI, AgCl, and CuBr Using Kelvin Probe Technique with Different Kinds of Probes. *J. Exp. Theor. Phys.* **2016**, *123* (1), 143–148.
- (18) Liu, C.-H.; Wu, C.-C.; Zhong, Z. A Fully Tunable Single-Walled Carbon Nanotube Diode. *Nano Lett.* **2011**, *11* (4), 1782–1785.
- (19) Suzuki, D.; Ochiai, Y.; Nakagawa, Y.; Kuwahara, Y.; Saito, T.; Kawano, Y. Fermi-Level-Controlled Semiconducting-Separated Carbon Nanotube Films for Flexible Terahertz Imagers. *ACS Appl. Nano Mater.* **2018**, *1* (6), 2469–2475.
- (20) MacLeod, B. A.; Stanton, N. J.; Gould, I. E.; Wesenberg, D.; Ihly, R.; Owczarczyk, Z. R.; Hurst, K. E.; Fewox, C. S.; Folmar, C. N.; Holman Hughes, K.; Zink, B. L.; Blackburn, J. L.; Ferguson, A. J. Large N- and p-Type Thermoelectric Power Factors from Doped Semiconducting Single-Walled Carbon Nanotube Thin Films. *Energy Environ. Sci.* **2017**, *10* (10), 2168–2179.
- (21) Sloan, J.; Monthieux, M. Filled Carbon Nanotubes: (X@CNTs). In *Carbon Meta-Nanotubes*; John Wiley & Sons: Chichester, U.K., 2011; pp 225–271.
- (22) Tonkikh, A. A.; Tsebro, V. I.; Obraztsova, E. A.; Rybkovskiy, D. V.; Orekhov, A. S.; Kondrashov, I. I.; Kauppinen, E. I.; Chuvilin, A. L.; Obraztsova, E. D. Films of Filled Single-Wall Carbon Nanotubes as a New Material for High-Performance Air-Sustainable Transparent Conductive Electrodes Operating in a Wide Spectral Range. *Nanoscale* **2019**, *11* (14), 6755–6765.
- (23) Kang, S. D.; Snyder, G. J. Charge-Transport Model for Conducting Polymers. *Nat. Mater.* **2017**, *16* (2), 252–257.
- (24) Dörling, B.; Sandoval, S.; Kankla, P.; Fuertes, A.; Tobias, G.; Campoy-Quiles, M. Exploring Different Doping Mechanisms in Thermoelectric Polymer/Carbon Nanotube Composites. *Synth. Met.* **2017**, *225*, 70–75.
- (25) Yarali, M.; Hao, J.; Khodadadi, M.; Brahmi, H.; Chen, S.; Hadjiev, V. G.; Jung, Y. J.; Mavrokelos, A. Physisorbed versus Chemisorbed Oxygen Effect on Thermoelectric Properties of Highly Organized Single Walled Carbon Nanotube Nanofilms. *RSC Adv.* **2017**, *7* (23), 14078–14087.
- (26) Nakai, Y.; Honda, K.; Yanagi, K.; Kataura, H.; Kato, T.; Yamamoto, T.; Maniwa, Y. Giant Seebeck Coefficient in Semiconducting Single-Wall Carbon Nanotube Film. *Appl. Phys. Express* **2014**, *7* (2), 025103.
- (27) Hung, N. T.; Nugraha, A. R. T.; Hasdeo, E. H.; Dresselhaus, M. S.; Saito, R. Diameter Dependence of Thermoelectric Power of Semiconducting Carbon Nanotubes. *Phys. Rev. B: Condens. Matter Mater. Phys.* **2015**, *92* (16), 165426.
- (28) Huang, W.; Tokunaga, E.; Nakashima, Y.; Fujigaya, T. Thermoelectric Properties of Sorted Semiconducting Single-Walled Carbon Nanotube Sheets. *Sci. Technol. Adv. Mater.* **2019**, *20* (1), 97–104.
- (29) Moiala, A.; Nasibulin, A. G.; Brown, D. P.; Jiang, H.; Khriachtchev, L.; Kauppinen, E. I. Single-Walled Carbon Nanotube Synthesis Using Ferrocene and Iron Pentacarbonyl in a Laminar Flow Reactor. *Chem. Eng. Sci.* **2006**, *61* (13), 4393–4402.
- (30) Tonkikh, A. A.; Tsebro, V. I.; Obraztsova, E. A.; Suenaga, K.; Kataura, H.; Nasibulin, A. G.; Kauppinen, E. I.; Obraztsova, E. D. Metallization of Single-Wall Carbon Nanotube Thin Films Induced by Gas Phase Iodination. *Carbon* **2015**, *94*, 768–774.
- (31) Eremina, V. A.; Obraztsov, P. A.; Fedotov, P. V.; Chernov, A. I.; Obraztsova, E. D. Separation and Optical Identification of Semiconducting and Metallic Single-Walled Carbon Nanotubes. *Phys. Status Solidi B* **2017**, *254* (5), 1600659.
- (32) Kleshch, V. I.; Eremina, V. A.; Serbun, P.; Orekhov, A. S.; Lützenkirchen-Hecht, D.; Obraztsova, E. D.; Obraztsov, A. N. A Comparative Study of Field Emission From Semiconducting and Metallic Single-Walled Carbon Nanotube Planar Emitters. *Phys. Status Solidi B* **2018**, *255* (1), 1700268.
- (33) Tonkikh, A. A.; Obraztsova, E. A.; Obraztsova, E. D.; Belkin, A. V.; Pozharov, A. S. Optical Spectroscopy of Iodine-Doped Single-Wall Carbon Nanotubes of Different Diameter. *Phys. Status Solidi B* **2012**, *249* (12), 2454–2459.
- (34) Li, L.-J.; Khlobystov, N.; Wiltshire, J. G.; Briggs, G. A. D.; Nicholas, R. J. Diameter-Selective Encapsulation of Metallocenes in Single-Walled Carbon Nanotubes. *Nat. Mater.* **2005**, *4* (6), 481–485.
- (35) Fedotov, P. V.; Tonkikh, A. A.; Obraztsova, E. A.; Nasibulin, A. G.; Kauppinen, E. I.; Chuvilin, A. L.; Obraztsova, E. D. Optical Properties of Single-Walled Carbon Nanotubes Filled with CuCl by Gas-Phase Technique. *Phys. Status Solidi B* **2014**, *251* (12), 2466–2470.
- (36) Tsebro, V. I.; Tonkikh, A. A.; Rybkovskiy, D. V.; Obraztsova, E. A.; Kauppinen, E. I.; Obraztsova, E. D. Phonon Contribution to Electrical Resistance of Acceptor-Doped Single-Wall Carbon Nanotubes Assembled into Transparent Films. *Phys. Rev. B: Condens. Matter Mater. Phys.* **2016**, *94* (24), 245438.
- (37) Rao, A. M.; Eklund, P. C.; Bandow, S.; Thess, A.; Smalley, R. E. Evidence for Charge Transfer in Doped Carbon Nanotube Bundles from Raman Scattering. *Nature* **1997**, *388* (6639), 257–259.
- (38) Zhao, Y.; Wei, J.; Vajtai, R.; Ajayan, P. M.; Barrera, E. V. Iodine Doped Carbon Nanotube Cables Exceeding Specific Electrical Conductivity of Metals. *Sci. Rep.* **2011**, *1* (1), 83.
- (39) Shiraishi, M.; Ata, M. Work Function of Carbon Nanotubes. *Carbon* **2001**, *39* (12), 1913–1917.
- (40) Zhukov, A. A.; Gartman, V. K.; Borisenko, D. N.; Chernysheva, M. V.; Eliseev, A. A. Measurements of Work Function of Pristine and

- CuI Doped Carbon Nanotubes. *J. Exp. Theor. Phys.* **2009**, *109* (2), 307–313.
- (41) Yamamoto, H.; Seki, K.; Mori, T.; Inokuchi, H. Ultraviolet Photoelectron Spectroscopy of Solid Iodine. *J. Chem. Phys.* **1987**, *86* (4), 1775–1779.
- (42) Goldmann, A.; Westphal, D. Band Structure and Optical Properties of CuCl: An Angle-Resolved Study of Secondary Electron Emission. *J. Phys. C: Solid State Phys.* **1983**, *16* (7), 1335–1343.
- (43) Fukumaru, T.; Fujigaya, T.; Nakashima, N. Development of N-Type Cobaltocene-Encapsulated Carbon Nanotubes with Remarkable Thermoelectric Property. *Sci. Rep.* **2015**, *5*, 7951.
- (44) Chan, C. K.; Kahn, A.; Zhang, Q.; Barlow, S.; Marder, S. R. Incorporation of Cobaltocene as an N-Dopant in Organic Molecular Films. *J. Appl. Phys.* **2007**, *102* (1), 014906.
- (45) Lu, J.; Nagase, S.; Yu, D.; Ye, H.; Han, R.; Gao, Z.; Zhang, S.; Peng, L. Amphoteric and Controllable Doping of Carbon Nanotubes by Encapsulation of Organic and Organometallic Molecules. *Phys. Rev. Lett.* **2004**, *93* (11), 116804.
- (46) Eliseev, A. A.; Yashina, L. V.; Verbitskiy, N. I.; Brzhezinskaya, M. M.; Kharlamova, M. V.; Chernysheva, M. V.; Lukashin, A. V.; Kiselev, N. A.; Kumskov, A. S.; Freitag, B.; Generalov, A. V.; Vinogradov, A. S.; Zubavichus, Y. V.; Kleimenov, E.; Nachtegaal, M. Interaction between Single Walled Carbon Nanotube and 1D Crystal in CuX@SWCNT (X = Cl, Br, I) Nanostructures. *Carbon* **2012**, *50* (11), 4021–4039.
- (47) Fedotov, P. V.; Eremina, V. A.; Tonkikh, A. A.; Chernov, A. I.; Obratsova, E. D. Enhanced Optical Transparency of Films Formed from Sorted Metallic or Semiconducting Single-Walled Carbon Nanotubes Filled with CuCl. *Phys. Status Solidi B* **2016**, *253*, 2400.
- (48) Sauer, M.; Shiozawa, H.; Ayala, P.; Ruiz-Soria, G.; Liu, X.; Chernov, A.; Krause, S.; Yanagi, K.; Kataura, H.; Pichler, T. Internal Charge Transfer in Metallicity Sorted Ferrocene Filled Carbon Nanotube Hybrids. *Carbon* **2013**, *59*, 237–245.
- (49) Farhat, H.; Son, H.; Samsonidze, G. G.; Reich, S.; Dresselhaus, M. S.; Kong, J. Phonon Softening in Individual Metallic Carbon Nanotubes Due to the Kohn Anomaly. *Phys. Rev. Lett.* **2007**, *99* (14), 1–4.
- (50) Sasaki, K.; Farhat, H.; Saito, R.; Dresselhaus, M. S. Kohn Anomaly in Raman Spectroscopy of Single Wall Carbon Nanotubes. *Phys. E* **2010**, *42* (8), 2005–2015.
- (51) Tsang, J. C.; Freitag, M.; Perebeinos, V.; Liu, J.; Avouris, P. Doping and Phonon Renormalization in Carbon Nanotubes. *Nat. Nanotechnol.* **2007**, *2* (11), 725–730.
- (52) Burstein, E. Anomalous Optical Absorption Limit in InSb. *Phys. Rev.* **1954**, *93* (3), 632–633.
- (53) Moss, T. S. The Interpretation of the Properties of Indium Antimonide. *Proc. Phys. Soc., London, Sect. B* **1954**, *67* (10), 775–782.
- (54) Kharlamova, M. V.; Yashina, L. V.; Volykhov, A. A.; Niu, J. J.; Neudachina, V. S.; Brzhezinskaya, M. M.; Zyubina, T. S.; Belogorokhov, A. I.; Eliseev, A. A. Acceptor Doping of Single-Walled Carbon Nanotubes by Encapsulation of Zinc Halogenides. *Eur. Phys. J. B* **2012**, *85* (1), 1–8.
- (55) Davis, E. A.; Mott, N. F. Conduction in Non-Crystalline Systems V. Conductivity, Optical Absorption and Photoconductivity in Amorphous Semiconductors. *Philos. Mag.* **1970**, *22* (179), 0903–0922.
- (56) Kim, S. L.; Choi, K.; Tazebay, A.; Yu, C. Flexible Power Fabrics Made of Carbon Nanotubes for Harvesting Thermoelectricity. *ACS Nano* **2014**, *8* (3), 2377–2386.
- (57) Tauc, J. *Amorphous and Liquid Semiconductors*; Tauc, J., Ed.; Springer: Boston, MA, 1974.
- (58) Li, X.; Zhu, H.; Wei, J.; Wang, K.; Xu, E.; Li, Z.; Wu, D. Determination of Band Gaps of Self-Assembled Carbon Nanotube Films Using Tauc/Davis–Mott Model. *Appl. Phys. A: Mater. Sci. Process.* **2009**, *97* (2), 341–344.
- (59) Skelton, E. F.; Webb, A. W.; Rachford, F. J.; Taylor, P. C.; Yu, S. C.; Spain, I. L. Investigations of the Pressure Dependence of Structural, Chemical, Electrical, and Magnetic Properties of Cuprous Chloride (CuCl). *Phys. Rev. B: Condens. Matter Mater. Phys.* **1980**, *21* (11), 5289–5296.
- (60) Vasquez, R. P. CuCl by XPS. *Surf. Sci. Spectra* **1993**, *2* (2), 138–143.
- (61) Vasquez, R. P. CuCl₂ by XPS. *Surf. Sci. Spectra* **1993**, *2* (2), 160–164.
- (62) Barreca, D.; Gasparotto, A.; Tondello, E. CVD Cu₂O and CuO Nanosystems Characterized by XPS. *Surf. Sci. Spectra* **2007**, *14* (1), 41–51.
- (63) Hung, N. T.; Nugraha, A. R. T.; Saito, R. Thermoelectric Properties of Carbon Nanotubes. *Energies* **2019**, *12* (23), 4561.
- (64) Blackburn, J. L.; Kang, S. D.; Roos, M. J.; Norton-Baker, B.; Miller, E. M.; Ferguson, A. J. Intrinsic and Extrinsic Limited Thermoelectric Transport within Semiconducting Single-Walled Carbon Nanotube Networks. *Adv. Electron. Mater.* **2019**, *5* (11), 1800910.
- (65) Hayashi, D.; Ueda, T.; Nakai, Y.; Kyakuno, H.; Miyata, Y.; Yamamoto, T.; Saito, T.; Hata, K.; Maniwa, Y. Thermoelectric Properties of Single-Wall Carbon Nanotube Films: Effects of Diameter and Wet Environment. *Appl. Phys. Express* **2016**, *9* (2), 025102.
- (66) Bubnova, O.; Khan, Z. U.; Wang, H.; Braun, S.; Evans, D. R.; Fabretto, M.; Hojati-Talemi, P.; Dagnelund, D.; Arlin, J.-B.; Geerts, Y. H.; Desbief, S.; Breiby, D. W.; Andreasen, J. W.; Lazzaroni, R.; Chen, W. M.; Zozoulenko, I.; Fahlman, M.; Murphy, P. J.; Berggren, M.; Crispin, X. Semi-Metallic Polymers. *Nat. Mater.* **2014**, *13* (2), 190–194.
- (67) Wang, X.; Wang, H.; Liu, B. Carbon Nanotube-Based Organic Thermoelectric Materials for Energy Harvesting. *Polymers (Basel, Switz.)* **2018**, *10* (11), 1196.
- (68) Jhi, S.-H.; Louie, S. G.; Cohen, M. L. Electronic Properties of Oxidized Carbon Nanotubes. *Phys. Rev. Lett.* **2000**, *85* (8), 1710–1713.
- (69) Chan, C. K.; Amy, F.; Zhang, Q.; Barlow, S.; Marder, S.; Kahn, A. N-Type Doping of an Electron-Transport Material by Controlled Gas-Phase Incorporation of Cobaltocene. *Chem. Phys. Lett.* **2006**, *431* (1–3), 67–71.
- (70) Rybkovskiy, D. V.; Impellizzeri, A.; Obratsova, E. D.; Ewels, C. P. Polyiodide Structures in Thin Single-Walled Carbon Nanotubes: A Large-Scale Density-Functional Study. *Carbon* **2019**, *142*, 123–130.